

Improved Synchronous Machine Thermal Modelling

Carlos Mejuto^{*}; Markus Mueller^{*}; Martin Shanel[°]; Adbeslam Mebarki[°]; Martin Reekie^{*}; Dave Staton[†]

^{*}The University of Edinburgh, School of Engineering and Electronics; [°]Cummins Generator Technologies; [†]Motor Design Ltd.
^{*}C.Mejuto@ed.ac.uk; [°]Martin.Shanel@Cummins.com; [†]Dave.Staton@Motor-Design.com

Abstract - It is well accepted nowadays that in synchronous machine design procedures thermal aspects should be weighed equally with electromagnetic issues and considered in an iterative manner. Synchronous machine thermal models are being constantly optimised and improved, and many design areas are well understood and documented. Even so, there are a number of thermal model design aspects that require significant further study and analysis. These aspects include accurate machine operational loss prediction, precise loss distribution, thermal model discretisation level issues and cooling air flow implications. They will be analysed in the paper, with future related investigations being identified.

I. INTRODUCTION

The traditional use of raw spread sheet, equivalent circuit based, thermal modelling packages is giving way to more accurate and reliable thermal modelling techniques. These techniques make use of powerful numerical analysis methods such as computational fluid dynamics (CFD) and finite element analysis (FEA), combining them with the fast computation times linked with analytical lumped circuit analysis. Extensive studies using CFD [1] and FEA [2] on numerous machine types and operating conditions have generated a high level of insight regarding the thermal behaviour of electrical machines, which is now taken into account in the creation of modern machine thermal models.

In practice, exclusive use of these accurate numerical design tools for all design queries and customer design checks would be impossible due to the tedious calibration and lengthy computing times required. This makes the need for precise analytically based thermal models even more pressing.

There are numerous benefits to be obtained from improved thermal models, ranging from the economical to the ecological. They will allow the rapid design of smaller, cooler, more efficient machines with a better overload capability, reduced running costs and a lesser environmental impact due to the associated reduction in operational losses. In addition, machines designed in this way will have significantly longer lifetimes, which will also bring obvious benefits to customers and manufacturers alike [3, 4].

II. IRON LOSS LAMINATION DISTRIBUTION

FEA is a powerful tool that can help designers model the magnetic flux distribution in machines more accurately. Iron losses and their distribution can then be calculated from such solutions. In order to predict these losses in an effective and reliable manner, harmonic evaluation of the flux density waveform in each FEA model element for the time cycle under investigation is required. Hence, the end result is a decomposition of the magnetic flux waveform per element into

its constituent parts (fundamental, 1st order, 2nd order, 3rd order, etc.).

For ferrite materials, this is then used to compute the loss per harmonic using the well-known Steinmetz formulae [5], shown in Equation 1.

$$\text{Iron Loss, } P_t = C_m f^\alpha B_m^\beta \tag{1}$$

where P_t is the total iron loss, and C_m , α and β are empirical parameters obtained from experimental measurement under sinusoidal conditions. B_m represents the peak magnetic flux density and f represents frequency.

More generally, total iron loss is the sum of the hysteresis and eddy current components, with the addition of an excess loss component due to domain wall effects, which should be taken into account for non-ferrite materials [6, 7, 8].

$$\text{Iron Loss, } P_t = P_h + P_e + P_x \tag{2}$$

$$= k_h f B_m^\beta + k_e (f B_m)^2 + k_x (f B_m)^{1.5} \tag{3}$$

where P_h is the hysteresis component, P_e the eddy-current component and P_x the excess loss. The constants k_h , k_e , k_x and β , are the respective loss constants and are determined by curve fitting to measured iron loss data.

Using FEA and iron loss equation (3) provides accurate predictions of losses, together with their distribution across the machine's cross-section [9]. An example for a 22.5 kVA, 31.3 A, 415 V, 50 Hz clockwise rotating machine is shown in Figure 1. This displays the magnetic flux distribution across the synchronous machine, which is closely linked iron loss magnitude and distribution.

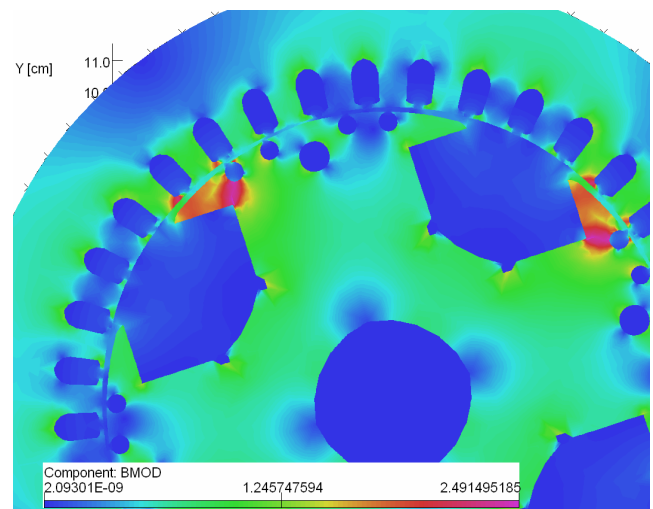


Figure 1: Alternator's magnetic flux density distribution.

The application of these losses to the generator’s thermal model results in a much more realistic temperature distribution.

Lumped thermal network coefficients can be derived by using the calculated loss data and comparing the iron loss concentration distribution across the machine. These coefficients have been called Lumped Circuit Coefficients (LCCs) and they greatly assist in the generation of a lumped circuit thermal model that is truly representative of the synchronous generator’s rotor and stator loss distribution. They are presented in the Figures 2 and 3.

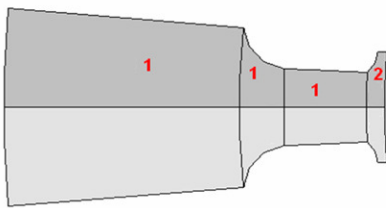
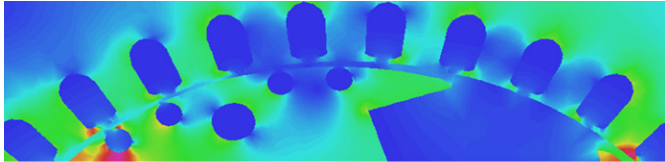


Figure 2: Stator loss coefficient distribution [10].

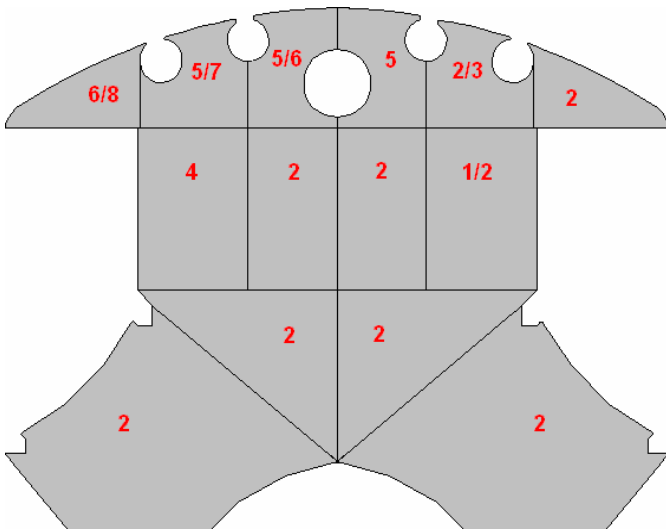


Figure 3: Rotor loss coefficient distribution [10].

The coefficients presented in Figure 3 are for the machine’s rotor lamination. They can be applied to the machine’s thermal model reluctance network as weighing factors, resulting in an improved synchronous generator thermal model that simulates the iron loss distribution of the alternator in a more realistic manner [10].

As well as giving the level and distribution of the iron losses, FEA can provide the total iron loss stator to rotor split ratio. Evaluation of a wide range of operating points reveal a stator:rotor iron loss split ratio of 85:15. This is a useful result

for machine designers as it allows a quick loss evaluation from overall loss figures.

III. ITERATIVE IRON LOSS CALIBRATION

A fundamental aspect of iron loss modelling involves the prediction of temperature variations at specific locations within a machine. In addition to the increase in accuracy achieved by using radial LCCs, the iron loss axial length distribution must also be considered. Machine losses will be more highly concentrated at the hotter sections of the generator and a reliable modelling package should take this into account. To achieve this, an iterative process was developed that updates iron losses with local component temperatures. Using this technique, a more realistic distribution of axial and radial temperatures is found. This method was applied to for the rotor and stator laminations models shown in Figure 4 and the results are presented in Reference [10].

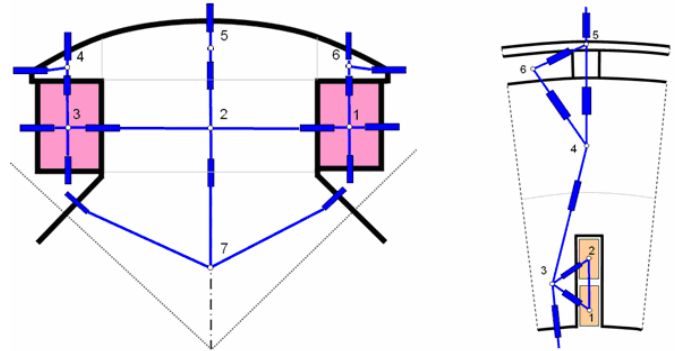


Figure 4: Rotor (left) & stator (right) lamination lumped networks.

A. Rotor lamination iron loss re-distribution

In the rotor a lumped parameter circuit is used. Iron losses are added at nodes 2, 4, 5, 6 and 7, shown in Figure 4, but only copper losses are fed into nodes 1 and 3. The iterative process utilises local temperatures in axial planes A, B and C (see Figure 6) to update iron losses.

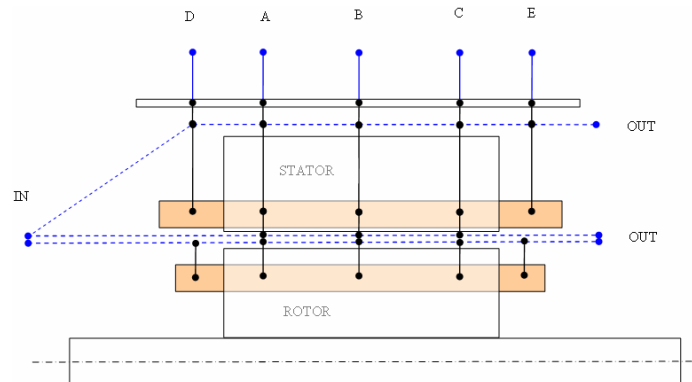


Figure 5: Axial planes in lumped parameter network.

These are updated according to a temperature ratio, which is initially assumed to be equally distributed between the three planes in Figure 5 (1/3 in each plane). The iterative process

proceeds until the change between updated input iron loss powers is less than 0.0001W between iterations. This can be adjusted depending on the level of accuracy desired. At this point a true axial temperature dependent iron loss rotor lamination distribution is achieved.

LCC results presented in Section 2 were combined with the axial temperature dependent iron loss iterative process and results for a full-load 22.5 kVA synchronous machine are shown in Figure 6. Series numbers 1 to 7 refer to rotor lamination nodes 1 to 7 in Figure 4. The results show that the application of LCCs allows for a realistic radial temperature distribution, which agrees with the FEA simulations that were also performed. Furthermore, in the axial direction, the iterative process yields hotter temperature spots towards the drive-end of the machine, as would be expected.

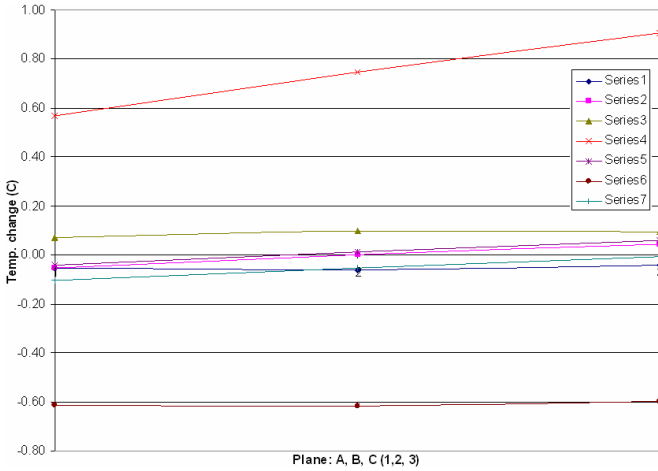


Fig. 6: Temperature dependent iron loss rotor lamination re-distribution results.

As can be seen, temperature changes within the rotor laminations of this machine are very small in magnitude. Even so, this is a useful step towards a more reliable thermal model and should be adopted. Furthermore, for bigger machines with higher kVA ratings, the temperature changes presented are significantly higher and so are more important if accurate predictions are required.

B. Stator lamination iron loss re-distribution

A similar method was applied to the stator lamination. In the stator a lumped parameter circuit is used and iron losses are only added to node 3, shown in Figure 4. Copper losses are fed into nodes 1 and 2. As before, the iterative process utilises local temperatures in axial planes A, B and C (see Figure 5) to update the iron losses. These are updated according to a temperature ratio, which is initially assumed to be equally distributed between the three planes (1/3 in each plane). The iterative process proceeds until the change between updated input iron loss powers is less than 0.0001W between iterations. At the completion of the iterative process a true axial temperature dependent iron loss stator lamination distribution is achieved.

Results are presented in Figure 7. Clearly temperature fluctuations in the axial direction are smaller than in the rotor

lamination and are therefore of a lesser importance. As with the rotor lamination simulation, results presented are for a full-load 22.5 kVA synchronous machine. Series numbers 1 to 6 refer to stator lamination nodes 1 to 6 in Figure 4.

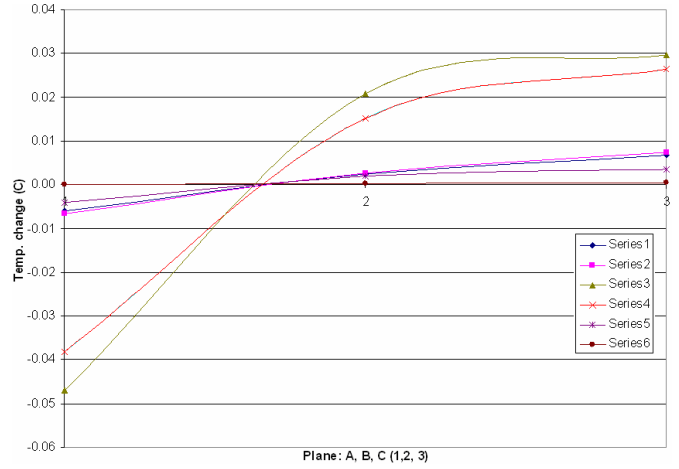


Fig. 7: Temperature dependent iron loss stator lamination re-distribution results.

IV. ROTOR WINDING DISCRETISATION STUDY

A thermal model’s discretisation level refers to the sections that are used to model the electrical machine, both in the axial and radial directions. The machine may be modelled as a whole, or only some of its more critical components may be involved. The level of discretisation employed in a thermal model is of great importance. An excessively crude model with too low a discretisation level will prove simple to create and fast to analyse, but will lack accuracy. On the other hand, increasing the discretisation level unjustifiably will complicate the model’s analysis without yielding better, more accurate results. Hence, it is critical that an acceptable discretisation level is identified, both in terms of accuracy and computing time.

The component’s thermal conductivity is the most important factor when determining discretisation levels for a thermal model. Structures made exclusively from components such as copper or steel would require very low discretisations due to their high thermal conductivities (around 400 Wm⁻¹K⁻¹ and 40 Wm⁻¹K⁻¹, respectively). Therefore, for example, heavily discretising a machine’s rotor lamination in the axial direction will bring little advantage, since heat travels with little obstruction in this direction. It is in the electrical machine’s windings where the use of a high discretisation level is very important. In the windings the conductivity is dramatically reduced by the presence of insulating resins (~0.25 Wm⁻¹K⁻¹) and trapped air pockets (~0.03 Wm⁻¹K⁻¹). Therefore, winding thermal conductivities fall to around 2-3 Wm⁻¹K⁻¹.

A study was performed in order to determine a reasonable axial discretisation level of a synchronous generator’s rotor and stator windings. To do this a number of rotor winding models were used, ranging from a ‘single block’ (1x1) representation to a detailed rotor winding model represented by 100 smaller

sections (10x10). The 1x1 and 10x10 models are illustrated in Figure 8.

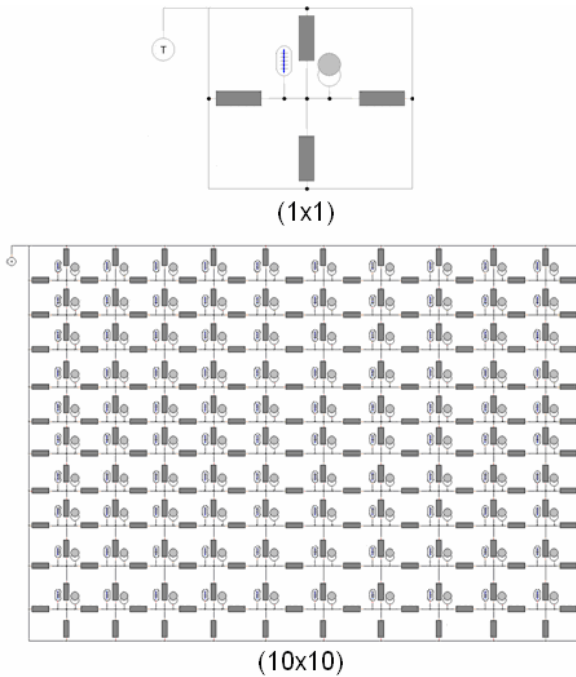


Figure 8: 1x1 (top) & 10x10 (bottom) rotor winding models.

An algorithm, to supply each discretisation model with the correct machine loss, was applied to each of the models considered. Algorithms were exposed to an identical loss scenario, with 1500 Watts of loss being divided between the power nodes making up the model, and the results obtained were graphed in Figure 9. At the same time FE thermal analysis (using CFD code Fluent) was used to analyse the winding under investigation, outputting an average winding stable state temperature of 17.07 °C. This temperature is the reference value used for the study in Figure 9.

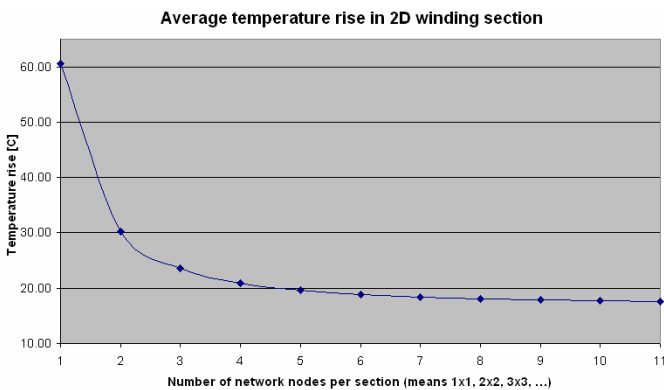


Figure 9: Rotor winding discretisation results up to 11x11.

As shown by the results, which were validated for a wide range of input losses, winding thermal conductivities and winding geometries, a rotor winding discretisation level of 10x10 yields very accurate results (17.71 °C) in comparison with the CFD results obtained. Using lower levels of discretisation reduces

the accuracy of the results, whilst increasing discretisation unnecessarily complicates the thermal model.

V. EXPERIMENTAL VALIDATION STAGE

Experimental work is required to shine some light on the thermal model ambiguities described in this paper. A synchronous generator will be fully thermally characterised in order to achieve an improved thermal model. To achieve this, an industry standard 22.5 kVA alternator has been fully equipped with numerous thermocouples along all thermally significant components (see Figure 10). Closely monitoring the generator heat runs for numerous operational conditions will provide a high level of insight on the machine's thermal behaviour.



Figure 10: Alternator thermal analysis test-rig set-up.

VI. ROTOR THERMOCOUPLE READING THROUGH SLIP-RINGS

The most challenging experimental section involves reading and processing the data from rotor thermocouples via shaft mounted bronze 11 brush slip-rings (see Figure 11). The main difficulty arises in the form of unintended thermocouple junctions. These can be reduced by ensuring that the correct thermocouple material wiring is utilised between the thermocouple sensors and the data acquisition system, but the junction located between the wiring and the slip-rings connections cannot be removed.

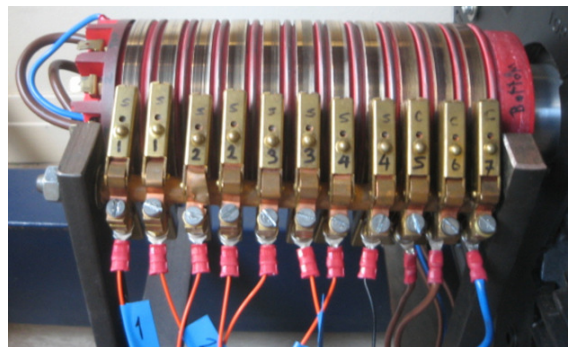


Figure 11: Shaft mounted bronze 11 brush slip-rings.

Furthermore, as the synchronous machine rotates at 1500rpm, the low voltage thermocouple readings (~0.8mV at 20 °C) can easily be swamped by electrical noise. Hence, it is vital that these signals are amplified as close to the source as possible and certainly prior to the slip-rings.

The material junction problem appears to be due to the frictional heat generated as the machine rotates, which causes the slip-rings to reach a temperature of ~60°C. The temperature difference between this junction and the temperature at the data acquisition end results in inaccurate results being collected. Although this junction cannot be removed since slip-rings are required, collecting, processing and amplifying the thermocouple voltages prior to the slip-rings will diminish the problem significantly, resulting in an acceptable level of accuracy.

To accomplish this, a small electronics PCB will be placed inside the slip-ring shaft. The PCB will read all 14 rotor winding thermocouples and process them through several multiplexers. In addition to this, an amplification stage will also be incorporated. A flow diagram of the electronics is shown in Figure 12.

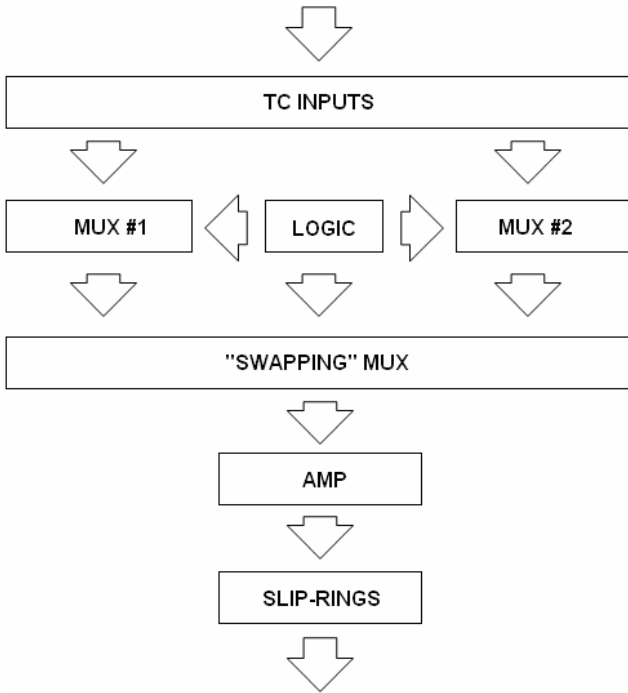


Figure 12: Flow diagram of rotor TC reading electronics.

The multiplexers (MUX), controlled by the logic stage will read each of the 14 rotor thermocouples in turn, whilst the amplification stage will increase the magnitude of the resulting multiplexer differential voltage before it is sent through the slip-ring to the data acquisition system. Though the output signal will still be susceptible to noise, the signal to noise ratio will be significantly increased. Protection circuitry will stop voltage spikes from saturating or damaging the multiplexers, and the inevitable 50 Hz noise will be cancelled and any remnants filtered out.

A crucial function of the electronics stage is performed by the “swapping” multiplexer. In order to remove slip-ring related temperature offsets, the following operation, outlined in Figure 13, is performed for every thermocouple reading. Two rings are allocated data output and these remain unchanged through the experimental stage to avoid introducing further offsets.

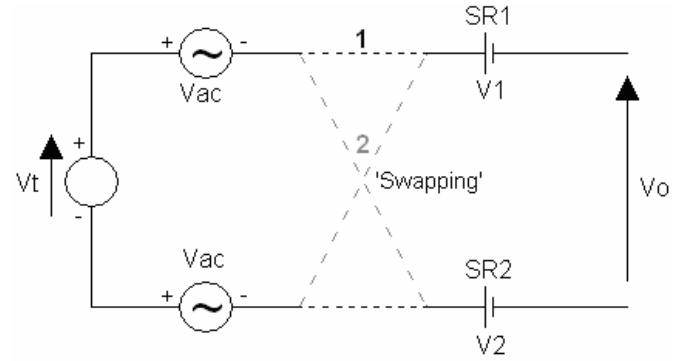


Figure 13: “Swapping” multiplexer operation.

where V_t is the thermocouple voltage, V_{ac} is the resulting ac voltage that generates on the thermocouple wires, V_1 is the voltage drop/offset through slip-ring 1 (SR1), V_2 is the voltage drop/offset through slip-ring 2 (SR2) and V_o is the resulting output voltage.

The ‘swapping’ dotted lines represent the possible reading paths allowed by the “swapping” MUX in Figure 13, paths 1 and 2. The “swapping” multiplexer takes one reading through path 1 and another through path 2 for every thermocouple measurement.

The ‘swapping’ procedure operates as follows. In general, analysing the circuit in Figure 13:

$$V_o = V_2 + V_{ac} + V_t - V_{ac} - V_1 \quad (4)$$

$$V_o = (V_2 - V_1) + V_t \quad (5)$$

Hence, V_o is obtained by the “swapping” multiplexer for the two positions shown in Figure 13. This yields V_{o1} and V_{o2} as shown.

$$V_{o1} = V_t + (V_2 - V_1) \quad (6)$$

$$V_{o2} = -V_t + (V_2 - V_1) \quad (7)$$

Therefore, a simple multiplexer subtraction of (6) and (7) removes the unwanted voltage offset introduced by the slip-rings.

$$V_{o1} - V_{o2} = 2V_t \quad (8)$$

Consideration was given to other data transmission systems, notably digitisation and radio transmission of the data, but that

would still require a scheme very similar to that outlined here to perform the necessary signal conditioning before digitisation and transmission. As the available space was extremely limited, this simpler system was used and found to be entirely adequate.

VII. FRAME & EXTERNAL THERMAL CAPTURES

In addition to the described work, an accurate thermal camera was used to obtain the machine's exterior thermal distribution. The comparison between the no-load and full-load machine external temperature distribution is shown in Figures 14 and 15. Agreeing with the results presented in Section 3, the drive-end of the machine is clearly at a higher temperature, with the drive-end end-caps and couplings the hottest.

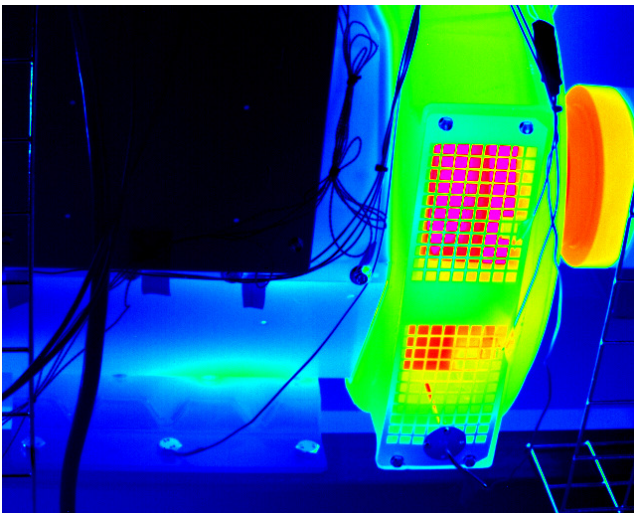


Figure 14: Alternator no-load thermal capture.

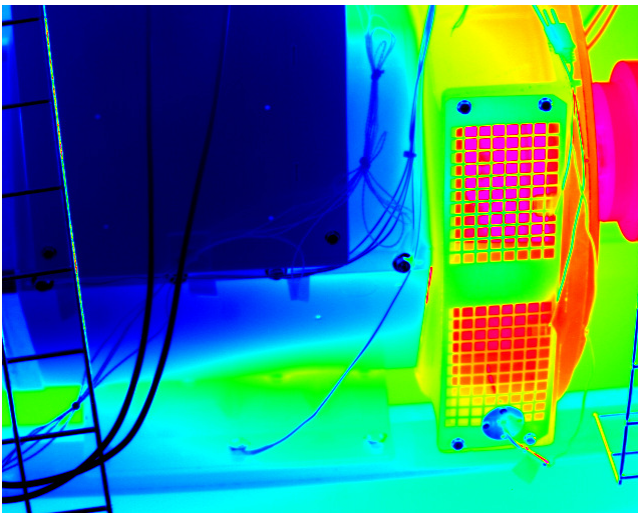


Figure 15: Alternator full-load thermal capture.

In Figures 14 and 15, the cooler blue shade of the non-drive-end of the machine is at $\sim 38^{\circ}\text{C}$, the warmer green/yellow drive-end is at $\sim 48^{\circ}\text{C}$ and the hottest end-cap sections are at $\sim 55^{\circ}\text{C}$.

VIII. FURTHER WORK

The method described in Section 6 allows for accurate thermal characterisation of the rotor winding. This, combined with the information collected from stator winding and frame thermocouples, will provide the complete machine thermal model desired. Initial simulations will then be confirmed, and the resulting thermal models will be validated over a wide range of operational conditions.

IX. CONCLUSIONS

The combined application of the thermal modelling improvements described in the paper has proven to result in more accurate and reliable synchronous machine thermal models. Additional experimental findings will further advance the current models, increasing accuracy and reliability. The models are applicable to a wide range of machines and ratings, aiding rapid effective operational consultations and easing new machine designs.

ACKNOWLEDGMENT

The authors thank The University of Edinburgh and Cummins Generator Technologies, as well as Motor Design Ltd. and Adapted Solutions for their aid and support.

REFERENCES

- [1] Maynes, B.D.J.; Kee, R.J.; Tindall, C.E.; Kenny, R.G.; "Simulation of airflow and heat transfer in small alternators using CFD", *Electric Power Applications, IEE Proceedings, Vol.150, No.2*, March '03 Page(s): 146-152.
- [2] Salon, S.J.; "Finite Element Analysis of Electrical Machines", *Rensselaer Polytechnic Institute, Kluwer Academic Publishers*.
- [3] Staton, D.; Pickering, S.J.; Lampard, D.; "Recent advancement in the thermal design of electric motors", *Paper presented at the SMMA 2001 Fall Technical Conference, Emerging Technologies for Electric Motion Industry*, Durham, North Carolina, USA, 3-5 October, 2001.
- [4] Al'Akayshee, Q.; Staton, D.A.; "1150hp Motor Design, Electromagnetic & Thermal Analysis", *ICEM, Brugge, Belgium*, 25-28 August, 2002.
- [5] Lin, D.; Zhou, P.; Fu, W. N.; Badics, Z.; Cendes, Z. J.; "A dynamic core loss model for soft ferromagnetic and power ferrite materials in transient finite element analysis", *IEEE Transactions on Magnetics, Vol.40, No. 2*, March 2004.
- [6] Mueller, M.A.; Williamson, S.; Flack, T.J.; Atallah, K.; Baholo, B.; Howe, D.; Mellor, P.H.; "Calculation of iron losses from time-stepped finite-element models of cage induction machines", *Electrical Machines and Drives, 1995. Seventh International Conference on (Conf. Publ. No. 412)*, 11-13 Sep. 1995, Page(s): 88.
- [7] Novinschi, A.; Brown, N.L.; Mebarki, A.; Haydock, L.; "The development of an FEA design environment model and comparison with traditional design and test data for the design of electrical machine", *IEE Conference on Power Electronics and Machines*, pp 574-572, 16-18 April 2002.
- [8] Brown, N.L.; Mebarki, A.; Hydock, L.; "Design aspect of a 200KW, 3600 rpm, permanent magnet generator for use in variable speed integrated generator", *IEE International Conference on Power Electronics and Machines*, pp 574-579, 16-18 April 2002.
- [9] Mueller, M.A.; Williamson, S.; McClay, C.I.; "Calculation of high-frequency losses in closed-slot induction motor rotors".
- [10] Mejuto, C.; Mueller, M.; Shanel, M.; Mebarki, A.; Staton, D.; "Thermal modelling investigation of heat paths due to iron losses in synchronous machines", *4th International Conference on Power Electronics, Machines and Drives*, - 4 April 2008, York St John University College, York, UK.